# Mechanochemical Reduction and Doping of Cobalt (II,III) Oxide ($Co_3O_4$) by Lithium Metal: A Facile Route to $Li_xCo_yO$ Materials

Nathan Davison[a], Isabel Arce-Garcia[b], Jamie A. Gould*[b], James A. Dawson*[a,d], Erli Lu*[a]

[a] Chemistry – School of Natural and Environmental Sciences, Newcastle University, Newcastle upon Tyne, UK

[b] Faculty of Sciences, Agriculture and Engineering, Newcastle University, Newcastle upon Tyne, UK

[c] School of Engineering, Newcastle University, Newcastle upon Tyne, UK

[d] Centre for Energy, Newcastle University, Newcastle upon Tyne, UK

*KEYWORDS: Mechanochemistry, Lithium, Cobalt Oxide, Doping, Reduction, Li-ion Batteries, Cathode Materials*

**ABSTRACT:** The reduction and doping of transition-metal oxides ($MO_x$) are essential processes in battery materials manufacturing, heterogeneous catalysis and metallurgy. However, due to the stability and inertness of $MO_x$, their reduction and doping are energetically demanding, requiring high temperature and/or a strong electro-potential. In this work, by introducing lithium metal as both a reductant and Li-ion source, we report the facile (10–15 minutes at room temperature) reduction and doping of cobalt (II,III) oxide ($Co_3O_4$) under mechanochemical conditions, to produce lithium-doped cobalt oxides ($Li_xCo_yO$) and cobalt metal. Reactions at different stoichiometric ratios are studied in one-pot and stepwise manners. Our combined experimental–computational analysis reveals the strongly exothermic profile of these reactions and proves that higher lithium contents in $Li_xCo_yO$ materials are achievable by conducting the reaction in a stepwise manner. This work provides a facile route for the reduction of $Co_3O_4$ and its Li doping to producing $Li_xCo_yO$ and $LiCoO_2$ battery cathode materials, which can only currently be made under energy- and carbon-intensive conditions (high temperatures for several hours).

Transition-metal oxides ($MO_x$) play essential roles in materials science and catalysis. Reduction and doping are two crucial processes to enable and improve the performance of $MO_x$-based materials and catalysts. Therefore, enormous research effort has been invested into these fields, from the chemical research communities [1] and beyond [2]. However, $MO_x$ materials feature thermodynamically stable lattice structures, rendering their reduction and doping processes energetically demanding and with harsh conditions required.

For example, cobalt (II,III) oxide ($Co_3O_4$) is widely applied in Li-ion battery (LIB) materials [3], catalysis [4] and gas sensors [5]. In LIB research, $Co_3O_4$ serves as an anode material, as well as a starting material to manufacture one of the most important LIB cathode materials: lithium cobalt oxide ($LiCoO_2$, LCO) [6]. $Co_3O_4$ is also an important source of Co metal through its reduction by the aluminothermic reaction or with carbon in a blast furnace [7]. In these applications, reduction and doping (e.g., $Li^+$ doping) play crucial and irreplaceable roles [8]. However, $Li^+$ doping of $Co_3O_4$ only occurs at > 600 °C over a duration of hours [6]. Comparably, the reduction of $Co_3O_4$ to Co metal [7] also only occurs under extreme conditions, such as under reducing atmosphere (hydrogen/methane/ethanol) at 800–1100 °C [9,10], with hydrogen plasma at >800 K [11], or at the nano-scale under strongly electrochemical reduction conditions [12]. Facile (room temperature and short reaction times) $Co_3O_4$ reduction and $Li^+$ doping at preparative scales are highly desirable, as they could potentially pave the way for new low-carbon and sustainable routes toward LIB materials (e.g., LCO) and Co metal. However, to the best of our knowledge, such facile $Co_3O_4$ reduction and doping reactions are currently unknown.

Mechanochemistry exploits mechanical forces (impact, shearing and pressing) to directly promote chemical transformations [13]. Compared to conventional solution-phase (stirring and heating) and solid-phase (high-temperature calcination) chemical synthetic methods, mechanochemistry features solvent-free and energy efficacy advantages. Mechanochemistry has a long history [14], with humans unintentionally using grinding to deliver chemistry in the prehistoric ages. This research field had been in hibernation until the 2000s, but the last two decades have witnessed a renaissance and upsurge in mechanochemistry research, driven mainly by the demands for low-carbon, sustainable and energy-efficient chemical synthesis methods [15]. Since then, mechanochemical methods have been used for organic [16], inorganic/organometallic [17], polymer [18] and supramolecular [19] chemistry. With regards to materials science, mechanochemical methods have also been employed to synthesize metal oxide nanoparticles [20] and prepare battery materials [21]. However, there is currently no precedent for using mechanochemical methods to promote the facile doping and reduction of metal oxides.

A recent Perspective from Pacchioni and co-workers suggested a strategy to increase the reducibility of $MO_x$ by increasing their interfacial areas [22]. In this regard, mechanochemical methods are perfectly suited for increasing the reducibility of $MO_x$, and therefore, promoting their facile reduction. However, this route has not been explored so far. In this context and based on our interest in lithium chemistry [23]-[25], we hypothesized that by introducing lithium metal as a reductant and a Li-ion source, and using mechanochemical methods to increase the reducibility of $Co_3O_4$, it is possible to deliver facile $Co_3O_4$ reduction and $Li^+$ doping in a one-pot manner. The findings are reported herein.

Lithium metal (ingots) and $Co_3O_4$ (powder) at three different stoichiometric ratios (Li:$Co_3O_4$ = 1:1, 2:1 or 3:1) (Scheme 1) were treated in a mechanochemical ball mill using an air-tight Teflon™ jar and a Teflon™-coated steel ball (see Supporting Information for details). We chose Teflon™ as the jar/ball material to avoid the formation of Li-Fe alloys during ball milling. The ball milling frequency and time are key factors that influence the reaction outcomes. We employ a mild 20 Hz frequency to avoid potential thermal runaway. The reactions were conducted in an intermittent manner by stopping the ball milling every 1 to 2 min to check the external temperature of the reaction jar. In all three reactions, we observed a 3 to 5 min induction period (jar temperature did not rise), followed by a 1 to 2 min exothermic reaction period (jar temperature increased to ~35–45 °C). The ball milling processes continued after the exothermic period until the total reaction times reached 15 min to ensure that the reactions were completed.

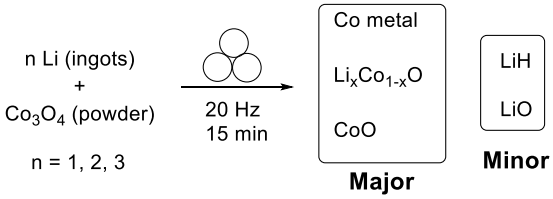


**Scheme 1.** Mechanochemical reactions between Li metal and $Co_3O_4$.

A 1:1 Li:$Co_3O_4$ reaction leads to the full consumption of Li metal ingots, producing a mixture of a black powder and hard metallic grains (average dimension of the metallic grains is ~2mm). Surprisingly, we found that the metallic grains were ferromagnetic and suspected to be Co metal, as confirmed by EDX SEM (*vide infra*). In terms of mass balance, 85 wt.% of the input materials was recovered (the rest of the materials stuck to the ball/jar surfaces and could not be retrieved), among which 20–25 wt.% was the Co metal grains and 75–80 wt.% was the black powder.

The black powder was analyzed by powder X-ray diffraction (PXRD) on a silicon zero-background sample holder. The PXRD result suggests that the main phase of the black powder was unreacted $Co_3O_4$, with a small amount of $Li_{0.19}Co_{0.81}O$ [26]-[28] and a second form of $Co_3O_4$ ($CoO{\cdot}Co_2O_3$) (Figure 1a). $Li_{0.19}Co_{0.81}O$ belongs to the family of Li-doped Co(II)O materials, formulated as $Li_xCo_{1-x}O$ ($0 < x < 0.2$) [26]-[28], which features a rock salt structure and have been widely investigated as precursors to the mainstream commercial Li-ion battery cathode material LCO [29]. From a structural perspective, $Li_xCo_{1-x}O$ is a solid solution of $Li^+$ in Co(II)O, with a mixed-valent Co(II,III) structure of general formula $Li_xCo(II)_{1-2x}Co(III)_xO$ [29]. To form the solid solution, the traditional method is to heat a mixture of $Li_2O_2$ ($Li^+$ source) and CoO at 900 °C [26]-[28]. In comparison, this work demonstrates that $Li_xCo_{1-x}O$ materials can be produced under mild mechanochemical conditions (room temperature for 15 min). It is also noteworthy that the powdery products from the 1:1 reaction are not sensitive to air, with their PXRD patterns identical under argon or air.

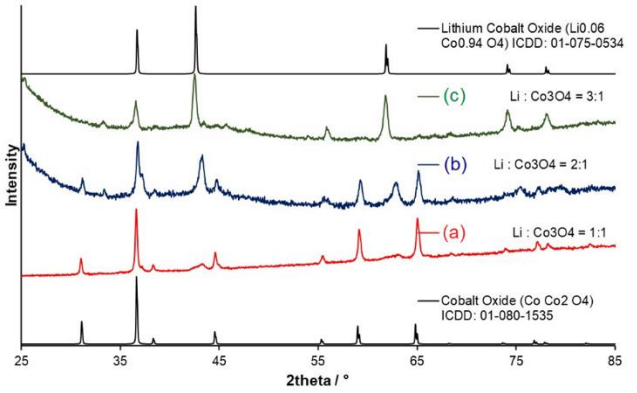


**Figure 1.** Powder X-ray diffraction data of the powdery products from the 1:1 (a, red), 2:1 (b, blue) and 3:1 (c, green) reactions, along with $Li_{0.06}Co_{0.94}O_4$ (ICDD 01-075-0534) (top) and $Co_3O_4$ (01-080-1535) (bottom) for comparison.

Since $Co_3O_4$ was in excess in the 1:1 reaction, we increased the Li:$Co_3O_4$ ratio to 2:1. Similar to the 1:1 reaction, we recovered ~85 wt.% of the materials, among which 35–40 wt.% was Co metal ingots and 60–65 wt.% was a black powder. The PXRD data of the powdery products from the 2:1 reaction indicates that the main phase was $Li_{0.185}Co_{0.815}O$, with a small quality of unreacted $Co_3O_4$ (less than for the 1:1 reaction) and $Li_2O$ (Figure 1b). It is noteworthy that the Co metal ingots increase in both weight percentage and grain size (6–8 mm) compared to the 1:1 reaction (Figure 2a).

The Co metal ingots were covered with a hard shell of black powder. Removal of the shell exposed metallic surfaces, which are stable in air for several days. EDX SEM data of multiple sites on the metallic surfaces (Figure 2b) confirmed an average >85 wt.% of cobalt. Small weight percentages of carbon (7–10 wt.%) and oxygen (2–3 wt.%) are consistently present, probably from the milling jar's Teflon™ material (for carbon) and the $Co_3O_4$ starting material (for oxygen).

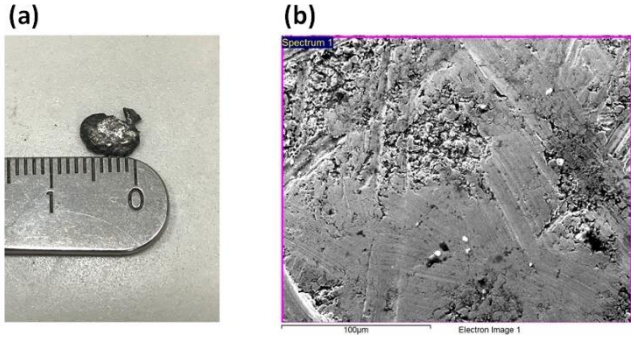

**Figure 2.** (a) An image of a cobalt metal ingot produced by the 2:1 Li:$Co_3O_4$ reaction (ball milling at 20 Hz for 15 min) after removal of the outer layer and polishing. (b) A representative EDX SEM image of the metallic surface (wt. %: C 7.6; O 8.9; Co 83.5). See Supporting Information for more EDX SEM images and analytical data.

Increasing the Li:$Co_3O_4$ ratio to 3:1 led to a mixture of Co metal ingots (15–20 wt.%) and a dark blue powder (80–85 wt.%). The dark blue powder was air sensitive, in contrast to the air-stable black powdery products from the 1:1 and 2:1 reactions. The PXRD data (collected under argon atmosphere) of the dark blue products indicates that it was a mixture of Co(II)O (main), $Li_{0.185}Co_{0.815}O$ (minor), Co (minor), Li (minor), LiH (minor) and $Li_2O$ (minor) (Figure 1c). There is no unreacted $Co_3O_4$, but instead, with the presence of unreacted Li.

An overview of the results from the 1:1, 2:1 and 3:1 reactions unveil two trends (Figure 3): (1) Co(II)O is only produced in the 3:1 reaction; (2) Co metal and $Li_xCo_{1-x}O$ increase from the 1:1 to the 2:1 reaction. The trends suggest that: (1) Co metal and $Li_xCo_{1-x}O$ may come from the same reaction(s), as their amounts increase simultaneously; (2) Co(II)O may be produced in different reaction(s) from which produced Co metal and $Li_xCo_{1-x}O$.

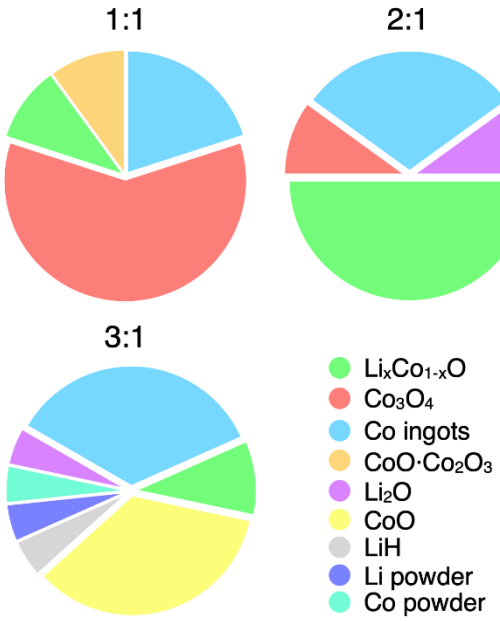


**Figure 3.** Approximate product concentrations (wt.%) for the 1:1, 2:1 and 3:1 Li:$Co_3O_4$ reactions.

In the literature, $Li_xCo_{1-x}O$ has been synthesized by oxidation reactions between $Li_2O_2$ and Co(II)O at 900 °C [26] [29]. In comparison, in our mechanochemical reactions, $Li_xCo_{1-x}O$ was formed by the reduction of $Co_3O_4$. Based on our observations, we hypothesize two competing reaction pathways (Figure 4): (1) Li(0) reduces part of the $Co_3O_4$ to Co(0), meanwhile $Li^+$ dopes into the remaining cobalt oxide, to form the $Li_xCo_{1-x}O$; (2) Li(0) reduces the $Co(II,III)_3O_4$ to Co(II)O and forms $Li_2O$. Pathway (1) dominates in the 1:1 and 2:1 reactions, while pathway (2) is favorable in the 3:1 reaction (Figure 4).

(1) $Li(0) + Co(II,III)_3O_4 \longrightarrow Li(I)_xCo(II)_{1-2x}Co(III)_xO + Co(0)$

(2) $Li(0) + Co(II,III)_3O_4 \longrightarrow Co(II)O + Li(I)_2O$

| Pathways \ Li:$Co_3O_4$ | 1:1 | 2:1 | 3:1 |
|---|---|---|---|
| (1) | ✓ | ✓ | |
| (2) | | | ✓ |

**Figure 4.** Two postulated competing reaction pathways, (1) and (2), and their preferences at different stoichiometric ratios. The stoichiometries of the reaction pathways are not balanced.

Density functional theory (DFT) calculations were used to verify this hypothesis and to further understand the reaction mechanisms between lithium metal and $Co_3O_4$. We began by calculating the total energies of the various reactants and products involved in the reactions between Li metal and $Co_3O_4$, including the low energy structures for $Li_xCo_{1-x}O$ (x = 0–0.44), as described in the Computational Details section of the Supporting Information. Based on the reactions proposed in Figure 4 and the reaction products measured in Figure 3, three possible fully balanced reactions are postulated (see Eqs. (S1–S9) in Supporting Information) for each of the three Li:$Co_3O_4$ ratios considered.

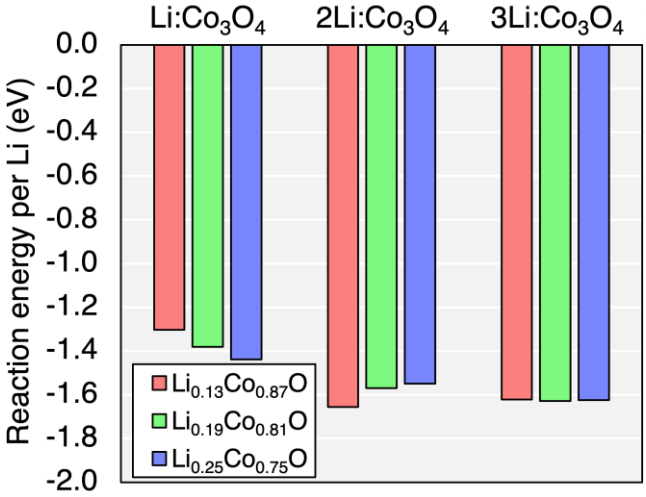


**Figure 5.** Calculated energies for reactions between Li metal and Li:$Co_3O_4$ as a function of the Li:$Co_3O_4$ ratio and Li doping concentration.

As expected, all the calculated reaction energies are strongly exothermic. It is noteworthy that the reactions energies for the three Li:$Co_3O_4$ ratios are reasonably similar, with values ranging from -1.30 to -1.63 eV per Li. Nevertheless, the most favorable reaction energy was found for the 2Li:$Co_3O_4$ ratio, in qualitative agreement with Figure 3. Furthermore, these results suggest that there is limited benefit in using high Li metal concentrations (i.e., 3Li:$Co_3O_4$) in these reactions as the energetic benefit per Li is negligible or is instead an energetic penalty. These findings support our postulated reaction mechanisms in Figure 4, where Li-doped CoO can be synthesized by the Li-facilitated reduction of $Co_3O_4$ to Co and Li doping into the remaining cobalt

oxide, or via the Li-facilitated reduction of $Co_3O_4$ to CoO and the formation of $Li_2O$.

With regards to the $Li^+$ doping concentration, each of the three reaction mechanisms displays a unique trend (Figure 5). For Li:$Co_3O_4$, the reaction energy increases with increasing Li, which suggests that, at least thermodynamically, higher Li concentrations in $Li_xCo_{1-x}O$ should be attainable. In contrast, the opposite trend is observed for 2Li:$Co_3O_4$, while in the case of 3Li:$Co_3O_4$, the reaction energy is unaffected by the Li dopant concentration considered. These results suggest that the reaction mechanism for Li metal and $Co_3O_4$ is likely to change based on the concentration of Li in $Li_xCo_{1-x}O$. A complete understanding of these mechanisms requires a range of factors, including reaction conditions and the interfaces of and between Li metal and $Co_3O_4$, to be accounted. Such simulations are currently being developed in our research groups and are expected to reveal crucial insights into the mechanochemistry of alkali metal and metal oxides.

For comparison, we also considered the energetics of the conventional solid-state reaction between $Li_2O_2$ and CoO used to synthesize $Li_xCo_{1-x}O$ [26–28]. As shown in Figure S6, the energies for this reaction, from -0.94 to -1.18 eV, are consistently less favorable than the reaction energies presented in Figure 5 for Li metal and $Co_3O_4$. This further evidences the potential of using Li metal as a starting material for the synthesis of lithium transition metal oxides materials.

To further understand the $Li^+$ doping process of CoO resulting from the reaction between Li metal and $Co_3O_4$ and to identify the character of the resulting reduced species, we carried out a Bader charge analysis [30] of the lowest energy $Li_xCo_{1-x}O$ configurations from the DFT calculations. Bader analysis has been previously used to investigate the charge states of numerous species in battery materials [31–33].

The results of the Bader charge analysis for Li, Co and O in $Li_xCo_{1-x}O$, as well as their percentage changes as a function of x, are presented in Figure S7. The greatest change in Bader charge (11.33%) as a result of increasing Li doping is found for O. In fact, the change in Bader charge for O is more than double the value obtained for Co (5.05%). The Bader charge of Li (~0.89 e) remains relatively constant at all doping concentrations. These findings suggest a significant level of oxygen oxidation (from –1.27 e at x = 0 to –1.14 e at x = 0.44), in addition to the expected Co oxidation (from 1.27 e at x = 0 to 1.33 e at x =0.44), as a result of Li doping CoO. Similar results have been observed previously using X-ray photoelectron spectroscopy for both the Li doping of CoO [34]and the deintercalation of Li from $LiCoO_2$ [35].

At x = 0–0.13 in $Li_xCo_{1-x}O$, the additional positive charge resulting from Li doping is localised on nearest neighbor O and second nearest neighbor Co sites to the Li dopants. This is illustrated by Figure S8 for $Li_{0.06}Co_{0.94}O$, where the doped Li ion forms three long (~2.41 Å) and three short (~2.03 Å) Li–O bonds with smaller and larger Bader charges, respectively. These longer Li–O bonds in turn result in shorter Co-O bonds (1.91 and 1.99 Å compared to ~2.11 Å in CoO) and a reduced charge for the adjacent Co ion. For x > 0.13, a mixture of Co and O charge states are found as a result of both localized and delocalized excess charge.

Our combined experimental and computational studies suggest that the formation of $Li_xCo_{1-x}O$ is preferable with a lower Li metal stoichiometric ratio. On this basis, it is sensible to extrapolate that, instead of a one-pot Li:$Co_3O_4$ 3:1 reaction, introducing the three equivalents of Li metal in a sequential manner would improve the production of $Li_xCo_{1-x}O$ (Figure 4, pathway 1), and suppresses pathway 2.

Indeed, we found that the sequential reaction not only increased the $Li_xCo_{1-x}O$ wt.%, but also produced doped materials with higher Li contents, such as $Li_{1.47}Co_3O_{3,72}$, $Li_{0.62}CoO_2$ and $LiCoO_2$ (Scheme 2), as postulated from the DFT analysis. In comparison, for the one-pot reactions, even with three equivalents of Li metal, the highest Li-content is $Li_{0.185}Co_{0.815}O$. The presence of unreacted Li-metal in the 3:1 one-pot reaction proved that the $Li_{0.185}Co_{0.815}O$ is probably the highest possible Li-content in the one-pot context. The limit, nonetheless, was broken by the sequential reactions, which achieve $Li_{0.62}CoO_2$ and $LiCoO_2$ (Scheme 2). We also noticed that, different from the one-pot reactions, the Co(II)O was not observed during the sequential reactions. The absence of Co(II)O corroborates our hypothesis of the two competing reaction pathways (Figure 4): Co(II)O would only be produced by pathway 2, which would only happen with excess Li metal. By conducting the reaction sequentially, the Li metal was not present in an excess amount at any moment, thereby suppressing pathway 2.

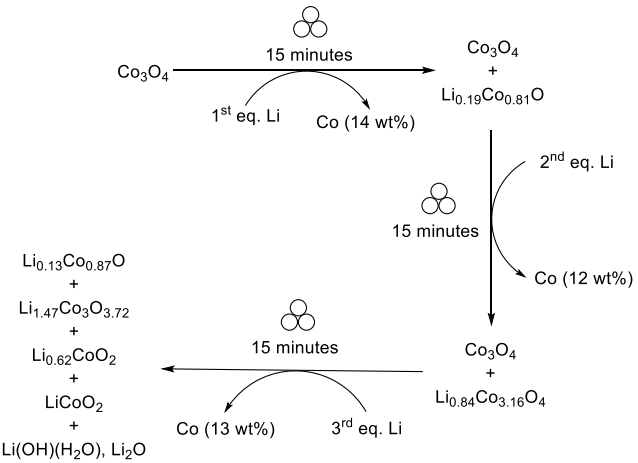


**Scheme 2.** Stepwise reactions between Li metal and $Co_3O_4$.

In conclusion, by utilizing a powerful experimental-computational approach, we have provided proof of concept for the use of Li metal as a highly efficient reductant and Li-ion source in a new low-carbon pathway to reduce inert $Co_3O_4$ and produce Co metal and $Li_xCo_{1-x}O$ mechanochemically. Compared to the state-of-the-art energy-intense manufacturing of $Li_xCo_{1-x}O$ and Co metal, this new mechanochemical approach features substantial potential in reducing the carbon footprint of cathode materials synthesis.

## ASSOCIATED CONTENT

**Supporting Information.**
Full experimental and computational details are included in the Supporting Information.

## AUTHOR INFORMATION

### Corresponding Authors

**Erli Lu –** Chemistry–School of Natural and Environmental Sciences, Newcastle University, Newcastle upon Tyne, UK. https://orcid.org/0000-0002-0619-5967. Email: Erli.Lu@newcastle.ac.uk

**James A. Dawson –** Chemistry–School of Natural and Environmental Sciences and Centre for Energy, Newcastle University, Newcastle upon Tyne, UK. Email: James.Dawson@newcastle.ac.uk

**Jamie A. Gould –** Faculty of Sciences, Agriculture and Engineering, Newcastle University, Newcastle upon Tyne, UK. Email: Jamie.Gould@newcastle.ac.uk

### Author Contributions

N. D. and E. L. designed and conducted the experiments. I. A. G. conducted the EDX SEM experiments and analyzed the data. J, A. D. designed and conducted the calculations and analyzed the data. J. A. G. conducted the PXRD experiments and analyzed the data. E. L. conceptualized the project, overviewed the research and wrote the manuscript with contributions of all authors.

## ACKNOWLEDGMENT

The authors thank the Newcastle University Chemistry Technical Support Team (Dr Laura McCorkindale, Dr Amy Roberts and Ms. Alexandra Rotariu) and Mr. Gary Day (Chemistry Mechanical Workshop) for supporting our research. E. L. thanks Profs. Steve Bull and Paul Christensen (School of Engineering, Newcastle University) for insightful discussions. E. L. and J. A. D. thank the Newcastle University Academic Track (NUAcT) Fellowship Scheme for financial support. N. D. thanks Newcastle University for a NUAcT PhD studentship. J.A.D. gratefully acknowledges the EPSRC (EP/V013130/1) for funding. Via membership of the UK's HEC Materials Chemistry Consortium, which is funded by the EPSRC (EP/L000202, EP/L000202/1, EP/R029431 and EP/T022213), this work used the ARCHER UK National Supercomputing Service. E. L. thanks the EPSRC North East Centre of Energy Materials (NECEM) and the Royal Society of Chemistry Research Enablement Grants (E20-5153) for financial support to build the mechanochemistry facility.

## REFERENCES

(1) Campbell, C. T.; Sauer, J. Introduction: Surface Chemistry of Oxides. *Chem. Rev.* **2013**, *113*, 3859–3862. DOI: 10.1021/cr4002337.

(2) Fang, F.; Kennedy, J.; Futter, J.; Markwitz, A.; Manikandan, E. Transition metal doped metal oxide nanostructures synthesized by arc discharge method. *2013 International Conference on Manipulation, Manufacturing and Measurement on the Nanoscale*, **2013**, pp. 220-223. DOI: 10.1109/3M-NANO.2013.6737418.

(3) Shi, Y.; Pan, X.; Li, B.; Zhao, M.; Pang, H. $Co_3O_4$ and its composites for high-performance Li-ion batteries. *Chem. Eng. J.* **2018**, *343*, 427-446. DOI: 10.1016/j.cej.2018.03.024.

(4) Xie, X.; Li, Y.; Liu, Z. -Q.; Heruta, M.; Shen, W. Low-temperature oxidation of CO catalyzed by $Co_3O_4$. *Nature* **2009**, *458*, 746-749. DOI: 10.1038/nature07877.

(5) Li, W. -Y.; Xu, L. -N.; Chen, J. $Co_3O_4$ Nanomaterials in Lithium-Ion Batteries and Gas Sensors. *Adv. Funct. Mater.* **2005**, *15*, 851-857. DOI: 10.1002/adfm.200400429.

(6) Shao-Horn, Y.; Croguennec, L.; Delmas, C.; Nelson, E. C.; O'Keefe, M. A. Atomic resolution of lithium ions in $LiCoO_2$. *Nature Mater.* **2003**, *2*, 464-467. DOI: 10.1038/nmat922.

(7) Holleman, A. F.; Wiberg, E.; Wiberg, N. (**2007**). "Cobalt" (in German). Lehrbuch der Anorganischen Chemie, 102nd Ed. de Gruyter. pp. 1146-1152. ISBN 978-3-11-017770-1.

(8) Garces, L. J.; Hincapie, B.; Zerger, R.; Suib, S. L. The Effect of Temperature and Support on the Reduction of Cobalt Oxide: An in situ X-ray Diffraction Study. *J. Phys. Chem. C* **2015**, *119*, 5484-5490. DOI: 10.1021/jp5124184.

(9) Khoshandam, B.; Kumar, R. V.; Jamshidi, E. Reduction of Cobalt Oxide with Methane. *Metall. Mater. Trans. B.* **2004**, 35b, 825-828. DOI: 10.1007/s11663-004-0076-7.

(10) Cetinkaya, S.; Eroglu, S. Synthesis of Cobalt Powder by Reduction of Cobalt Oxide with Ethanol. *JOM* **2018**, *70*, 2237-2242. DOI: 10.1007/s11837-018-2799-y.

(11) Sabat, K. C.; Paramguru, R. K.; Pradhan, S.; Mishra, B. K. Reduction of Cobalt Oxide ($Co_3O_4$) by Low Temperature Hydrogen Plasma. *Plasma Chem. Plasma Process* **2015**, *35*, 387-399. DOI: 10.1007/s11090-014-9602-9.

(12) Luo, L.; Wu, J.; Xu, J.; Dracid, V. P. Atomic Resolution Study of Reversible Conversion Reaction in Metal Oxide Electrodes for Lithium-Ion Battery. *ACS Nano* **2014**, *8*, 11560-11566. DOI: 10.1021/nn504806h.

(13) Do, J. –L.; Friščić, T. Mechanochemistry: A Force of Synthesis. *ACS Cent. Sci.* **2017**, *3*, 13-19. DOI: 10.1021/acscentsci.6b00277.

(14) Takacs, L. The historical development of mechanochemistry. *Chem. Soc. Rev.* **2013**, *42*, 7649-7659. DOI: 10.1039/C2CS35442J.

(15) Boldyreva, E. Mechanochemistry of inorganic and organic systems: what is similar, what is different? *Chem. Soc. Rev.* **2013**, *42*, 7719-7738. DOI: 10.1039/C3CS60052A.

(16) Friščić, T.; Mottillo, C.; Titi, H. M. Mechanochemistry for Synthesis. *Angew. Chem. Int. Ed.* **2020**, *59*, 1018-1029. DOI: 10.1002/anie.201906755.

(17) Rightmire, N. R.; Hanusa, T. P. Advances in organometallic synthesis with mechanochemical methods. *Dalton Trans.* **2016**, *45*, 2352-2362. DOI: 10.1039/C5DT03866A.

(18) Chen, Y.; Mellow, G.; van Luijk, D.; Creton, C.; Sijbesma, R. P. Mechanochemiscal tools for polymer materials. *Chem. Soc. Rev.* **2021**, *50*, 4100-4140. DOI: 10.1039/D0CS00940G.

(19) Rainer, D. N.; Morris, R. E. New avenues for Mechanochemistry in zeolite science. *Dalton Trans.* **2021**, *50*, 8995-9009. DOI: 10.1039/D1DT01440D.

(20) Tsuzuki, T. Mechanochemical synthesis of metal oxide nanoparticles. *Commun. Chem.* **2021**, *4*, 143. DOI: 10.1038/s42004-021-00582-3.

(21) Schlem, R.; Burmeister, C. F.; Michalowski, P.; Ohno, S.; Dewald, G. F.; Kwade, A.; Zeier, W. G. Energy Storage Materials for Solid-State Batteries: Design by Mechanochemistry. *Adv. Energy Mater.* **2021**, *11*, 2101022. DOI: 10.1002/aenm.202101022.

(22) Puigdollers, A. R.; Schlexer, P.; Tosoni, S.; Pacchioni, G. Increase Oxide Reducibility: The Role of Metal/Oxide Interfaces in the Formation of Oxygen Vacancies. *ACS Catal.* **2017**, *7*, 6493-6513. DOI: 10.1021/acscatal.7b01913.

(23) Davison, N.; Waddell, P. G.; Dixon, C.; Wills, C.; Penfold, T. J.; Lu, E. A monomeric (trimethylsilyl)methyl lithium complex: synthesis, structure, decomposition and preliminary reactivity studies. *Dalton Trans.* **2022**, DOI: 10.1039/d1dt03532k.

(24) Davison, N.; Falbo, E.; Waddell, P. G.; Penfold, T. J.; Lu, E. A monomeric methyllithium complex: synthesis and structure. *Chem. Commun.* **2021**, *57*, 6205-6208. DOI: 10.1039/D1CC01420J.

(25) Davison, N.; Zhou, K.; Waddell, P. G.; Wills, C.; Dixon, C.; Hu, S. –X.; Lu, E. Versatile Coordination Modes of Multidentate Neutral Amine Ligands with Group 1 Metal Cations. *Inorg. Chem.* **2022**, DOI: 10.1021/acs.inorgchem.1c03786.

(26) Johnston, W. D.; Heikes, R. R.; Sestrich, D. The Preparation, Crystallography, and Magnetic Properties of the $Li_xCo_{(1-x)}O$ System. *J. Phys. Chem. Solids* **1958**, *7*, 1–13. DOI: 10.1016/0022-3697(58)90175-6.

(27) Wu, Y.; Pasero, D.; McCabe, E. E.; Matsushima, Y.; West, A. R. Formation of disordered and partially ordered $Li_xCo_{1-x}O$. *J. Mater. Chem.* **2009**, *19*, 1443–1448. DOI: 10.1039/B816486J.

(28) Zehermaier, P. M.; Cornélis, A.; Zoller, F.; Böller, B.; Wisnet, A.; Döblinger, M.; Böhm, D.; Bein, T.; Fattakhova-Rohlfing, D. Nanosized Lithium-Rich Cobalt Oxide Particles and Their Transformation to Lithium Cobalt Oxide Cathodes with Optimized High-Rate Morphology. *Chem. Mater.* **2019**, *31*, 8685–8694. DOI: 10.1021/acs.chemmater.9b02231.

(29) Antolini, E. Phase transition of pure and Li-doped CoO on slow cooling from 1300 °C. *J. Phys. D: Appl. Phys.* **1998**, *31*, 334–335.

(30) Henkelman, G.; Arnaldsson, A.; Jonsson, H. A. Fast and Robust Algorithm for Bader Decomposition of Charge Density. *Comput. Mater. Sci.* **2006**, *36*, 354–360. DOI: 10.1016/j.commatsci.2005.04.010.

(31) Dawson, J. A.; Naylor, A. J.; Eames, C.; Roberts, M.; Zhang, W.; Snaith, H. J.; Bruce, P. G.; Saiful Islam, M. Mechanisms of Lithium Intercalation and Conversion Processes in Organic–Inorganic Halide Perovskites. *ACS Energy Lett.* **2017**, *2*, 1818–1824. DOI: 10.1021/acsenergylett.7b00437.

(32) Melot, B. C.; Scanlon, D. O.; Reynaud, M.; Rousse, G.; Chotard, J.-N.; Henry, M.; Tarascon, J.-M. Chemical and Structural Indicators for Large Redox Potentials in Fe-Based Positive Electrode Materials. *ACS Appl. Mater. Interfaces* **2014**, *6*, 10832–10839. DOI: 10.1021/am405579h.

(33) Xu, S.; Jacobs, R. M.; Nguyen, H. M.; Hao, S.; Mahanthappa, M.; Wolverton, C.; Morgan, D. Lithium Transport Through LithiumIon Battery Cathode Coatings. *J. Mater. Chem. A* **2015**, *3*, 17248–17272. DOI: 10.1039/C5TA01664A.

(34) van Elp, J.; Wieland, J. L.; Eskes, H.; Kuiper, P.; Sawatzky, G. A. Electronic structure of CoO, Li-doped CoO, and $LiCoO_2$. *Phys. Rev. B* **1991**, *44*, 6090-6103. DOI: 10.1103/PhysRevB.44.6090.

(35) Dahéron, L.; Dedryvère, R.; Martinez, H.; Ménétrier, M.; Denage, C.; Delmas, C.; Gonbeau, D. Electron Transfer Mechanisms upon Lithium Deintercalation from $LiCoO_2$ to $CoO_2$ Investigated by XPS. *Chem. Mater.* **2008**, *20*, 583-590. DOI: 10.1021/cm702546s.

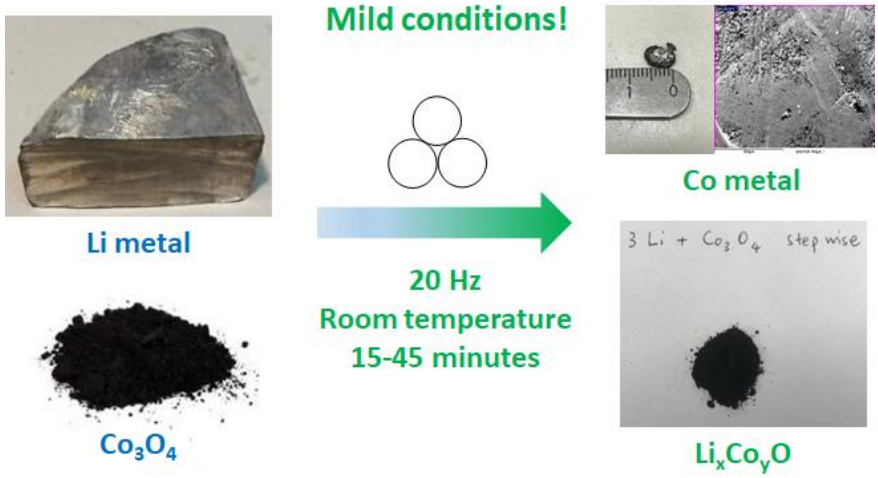


Insert Table of Contents artwork here